ELSEVIER

Ceramics International 31 (2005) 911–916

CERAMICS INTERNATIONAL

www.elsevier.com/locate/ceramint

# Thermal conductivity of zirconia–alumina composites

Narottam P. Bansal [a,*], Dongming Zhu [b]

[a] National Aeronautics and Space Administration, John H. Glenn Research Center at Lewis Field, Cleveland, OH 44135, USA
[b] U.S. Army, Vehicle Technology Directorate, Glenn Research Center, Cleveland, OH 44135, USA

Received 26 May 2004; received in revised form 26 August 2004; accepted 28 September 2004
Available online 20 March 2005

**Abstract**

Ten mole percent of yttria-stabilized zirconia (10YSZ)–alumina composites containing 0–30 mol% alumina were fabricated by hot pressing at 1500 °C in vacuum. Thermal conductivity of the composites, determined at various temperatures using a steady-state laser heat flux technique, increased with increase in alumina content. Composites containing 0, 5, and 10 mol% alumina did not show any change in thermal conductivity with temperature. However, those containing 20 and 30 mol% alumina showed a decrease in thermal conductivity with increase in temperature. The measured values of thermal conductivity were in good agreement with those calculated from the Maxwell–Eucken model where one phase is uniformly dispersed within a second major continuous phase.
Published by Elsevier Ltd and Techna Group S.r.l.

*Keywords:* B. Composites; C. Thermal conductivity; D. Zirconia; D. Alumina

## 1. Introduction

A fuel cell is an electrochemical device where the chemical energy of a fuel such as hydrogen is converted into electricity by electrochemical oxidation of the fuel. The only by-products of this process are water and heat. Various types of fuel cells (polymer electrolyte fuel cell, alkaline fuel cell, phosphoric acid fuel cell, methanol fuel cell, molten carbonate fuel cell, and solid oxide fuel cell) are being developed as power sources for a large number of applications. Solid oxide fuel (SOFC) cells [1] offer several advantages over other types of fuel cells such as high efficiency, low emissions, high power density, fuel flexibility, and internal fuel reforming. Yttria-stabilized zirconia (YSZ) is the most commonly used electrolyte for high-temperature SOFC because of its high oxide ion conductivity and stability in oxidizing and reducing atmospheres. However, like other ceramic materials, zirconia has low fracture toughness and poor strength. For aeropropulsion applications, the thin electrolyte membrane (10–50 μm thick) of the planar anode-supported SOFC needs to be strong and tough as it would be subjected to severe vibrations and thermal cycling during take-off and landing. It has been recently demonstrated [2–8] that the additions of alumina to 10YSZ make it stronger, tougher, lighter, and stiffer at room temperature as well as at 1000 °C. However, no information is available about the thermal conductivity of these composites. The objective of the present study was to investigate the effects of alumina additions on the thermal conductivity of 10YSZ in the SOFC operating temperature region.

## 2. Materials and experimental methods

The starting materials used were 10 mol% yttria fully-stabilized zirconia powder (HSY-10, average particle size 0.41 μm, specific surface area 5.0 $m^2$/g) from Daiichi Kigenso Kagaku Kogyo Co., Japan and alumina powder (Baikalox CR-30, 99.99% purity, average particle size 0.05 μm, specific surface area 25 $m^2$/g) from Baikowski International Corporation, Charlotte, NC. Appropriate quantities of 10YSZ powder and alumina powder were slurry mixed in acetone and ball milled for ∼24 h using zirconia milling media. Acetone was evaporated and the

* Corresponding author. Tel.: +1 216 433 3855; fax: +1 216 433 5544.
*E-mail address:* Narottam.P.Bansal@nasa.gov (N.P. Bansal).

0272-8842/$30.00. Published by Elsevier Ltd and Techna Group S.r.l.
doi:10.1016/j.ceramint.2004.09.018

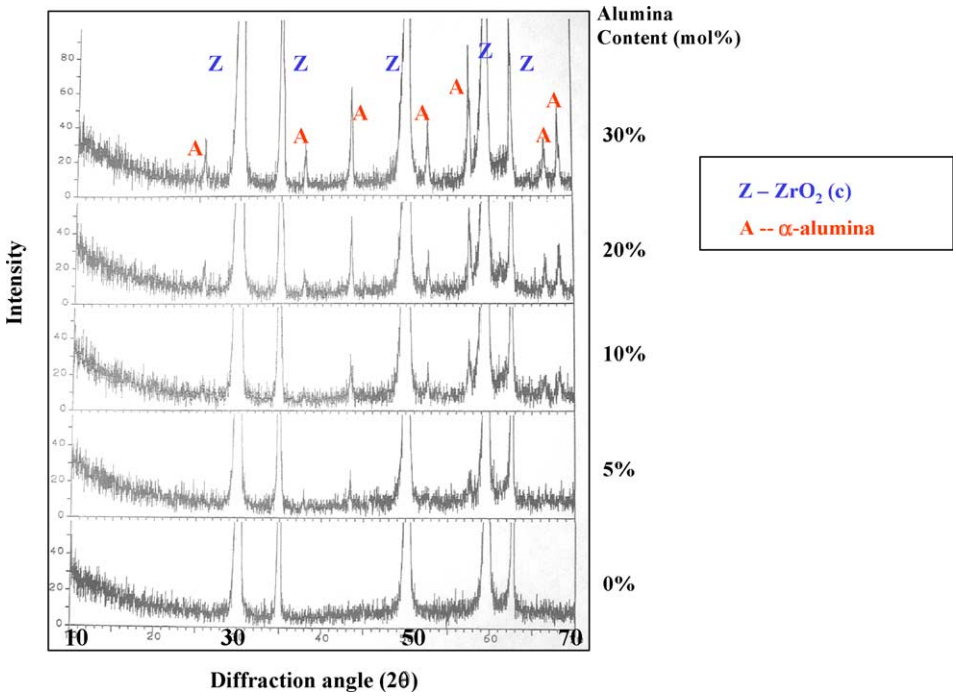


Fig. 1. X-ray diffraction patterns for 10YSZ reinforced with different alumina contents. "Z" and "A" indicate cubic-zirconia and α-alumina, respectively.

powder dried in an electric oven. The resulting powder was loaded into a graphite die and hot pressed at 1500 °C in vacuum under 30 MPa pressure into 1″ diameter discs using a mini-hot press. Grafoil was used as spacers between the specimen and the punches. Load was released before onset of cooling [2,4] after an isothermal hold at high temperature resulting in dense and crack-free ceramic composite samples. Residual grafoil from disc surfaces was burned off in air.

X-ray diffraction (XRD) patterns were recorded at room temperature using a step scan procedure (0.02/2$\theta$ step, count time 0.5 or 1 s) on a Philips ADP-3600 automated diffractometer equipped with a crystal monochromator employing Cu Kα radiation. Microstructures of the polished cross-sections of heat-treated glass specimens were observed using a JEOL JSM-840A scanning electron microscope (SEM). Qualitative X-ray elemental analysis of various phases was carried out using a Kevex Delta thin window energy dispersive spectrometer (EDS) and analyzer. Thin foils for transmission electron microscopy (TEM) were prepared using a procedure that involved slicing, polishing, and argon beam milling. The thin foils were examined in a Philips EM-400T operating at 120 keV. A thin carbon coating was evaporated onto TEM thin foils and SEM specimens for electrical conductivity.

## 3. Thermal conductivity measurement

One inch (25.4 mm) diameter hot-pressed discs of 10YSZ–alumina composites were used for thermal conductivity measurements. Thermal conductivity testing of the ceramic materials was carried out using a 3.0 kW $CO_2$ laser (wavelength 10.6 μm) high-heat flux rig. A schematic diagram of the test rig, photos of the actual test facilities and the general test approach have been described elsewhere [5]. In this steady-state laser heat flux test method, the specimen surface was heated by a laser beam, and backside air-cooling was used to maintain the desired temperature. A uniform laser heat flux was obtained over the 23.9 mm diameter aperture region of the specimen surface by using an integrating ZnSe lens combined with the specimen rotation. Platinum wire flat coils (wire diameter 0.38 mm) were used

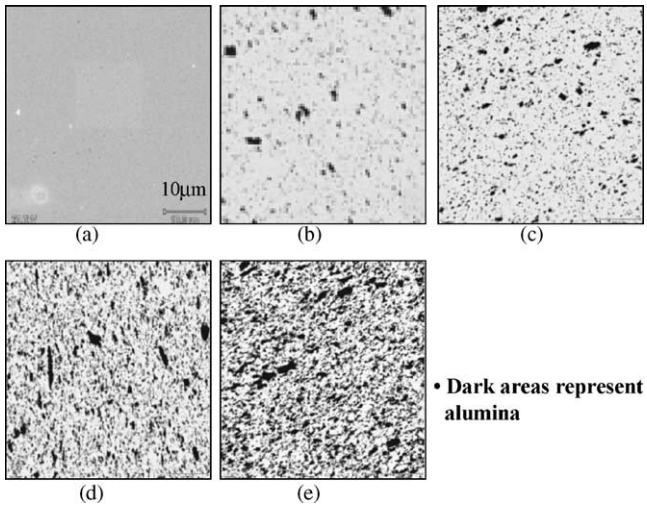


Fig. 2. SEM micrographs showing polished cross-sections of 10YSZ–alumina composites containing various alumina: (a) 0 mol%; (b) 5 mol%; (c) 10 mol%; (d) 20 mol%; (e) 30 mol%.

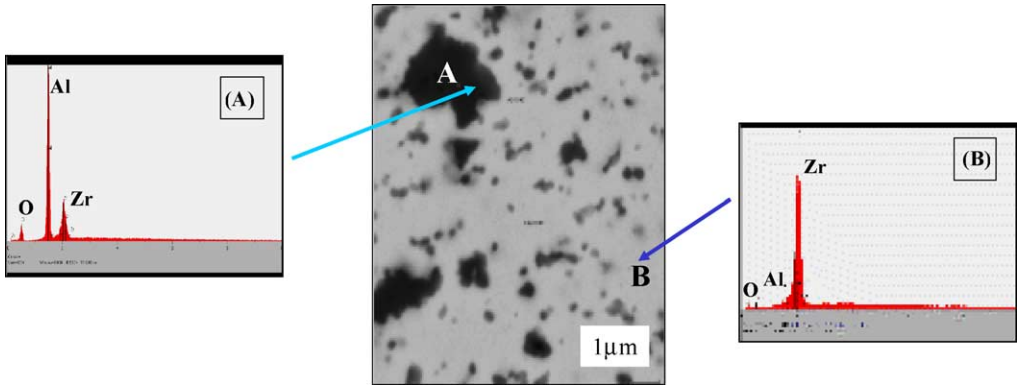


Fig. 3. SEM micrograph and EDS analysis of 10YSZ–alumina composite containing 10 mol% alumina: dark area (A): alumina, light area (B): zirconia.

to form thin air gaps between the top aluminum aperture plate and stainless-steel back plate to minimize the specimen heat losses through the fixture.

Thermal conductivity of ceramic materials, $k_{\text{ceramic}}$, can be determined from the pass-through heat flux $q_{\text{thru}}$ and measured temperature difference $\Delta T_{\text{ceramic}}$ across the ceramic specimen thickness $l_{\text{ceremic}}$ under the steady-state laser heating conditions [5]

$$k_{\text{ceramic}} = \frac{q_{\text{thru}} l_{\text{ceramic}}}{\Delta T_{\text{ceramic}}} \quad (1)$$

The actual pass-through heat flux $q_{\text{thru}}$ for a given ceramic specimen was obtained by subtracting the laser reflection loss (measured by a 10.6 μm reflectometer) and the calculated radiation heat loss (total emissivity was taken as 0.50 for the oxides) at the ceramic surface from the laser delivered heat flux (i.e., $q_{\text{thru}} = q_{\text{delivered}} - q_{\text{reflected}} - q_{\text{ra-radiated}}$). Note that the non-reflected laser energy is absorbed at or near the specimen surfaces because of the quite high emissivity at the 10.6 μm laser wavelength region for the oxides. In some test cases, the pass-through heat flux $q_{\text{thru}}$ was verified with an internal heat flux gauge incorporated with the substrates (instrumented specimens) via an embedded miniature thermocouple. For the hot-pressed bulk specimens, the temperature difference $\Delta T_{\text{ceramic}}$ in the ceramic was directly measured by using two 8 μm pyrometers at both specimen front heating and back-side air cooling surfaces.

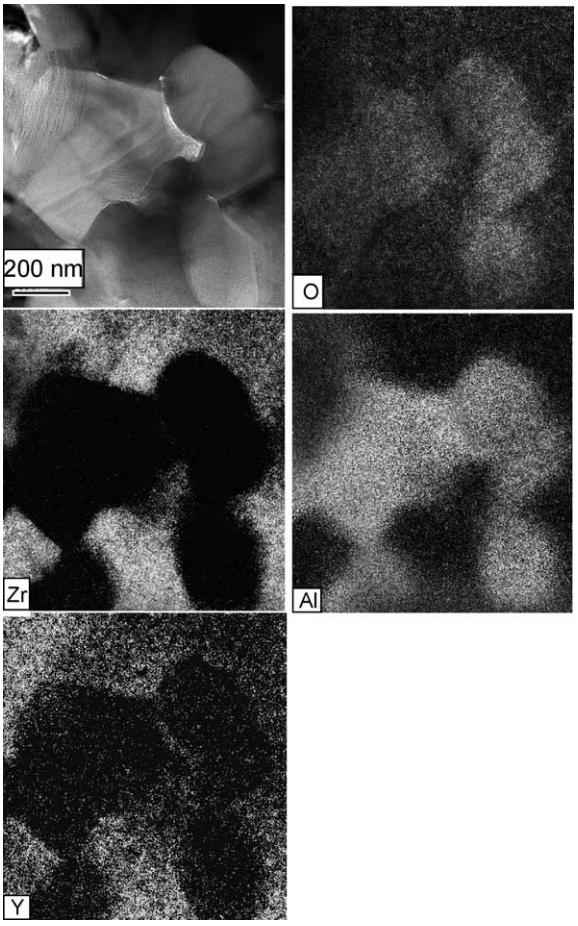


Fig. 4. TEM micrograph showing zirconia and alumina grains and dot maps of different elements for 10YSZ–alumina composite containing 30 mol% alumina.

## 4. Results and discussion

Compositions of various 10YSZ–alumina composites used in this study and their densities, $\rho$, are presented in Table 1. The specimens are at least 99% dense. Density decreased with increase in alumina content, as expected.

Table 1
Compositions of 10YSZ–alumina composites

| Sample number | Composition (mol%) | | Density, $\rho$ (g/cm$^3$) |
|---|---|---|---|
| | 10YSZ | $Al_2O_3$ | |
| A2-0 | 100 | 0 | 6.09 ± 0.05 |
| A2-5 | 95 | 5 | 5.89 ± 0.01 |
| A2-10 | 90 | 10 | 5.80 ± 0.01 |
| A2-20 | 80 | 20 | 5.57 ± 0.01 |
| A2-30 | 70 | 30 | 5.38 ± 0.04 |
| $Al_2O_3$ | 0 | 100 | 3.94 ± 0.03 |

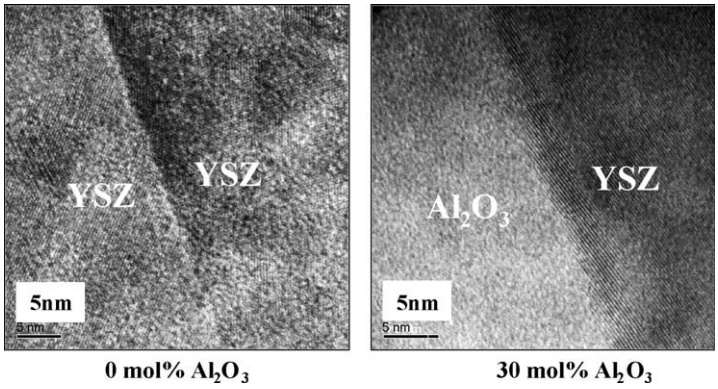


Fig. 5. High magnification TEM micrographs showing grain boundaries in 10YSZ–alumina composites containing 0 or 30 mol% alumina.

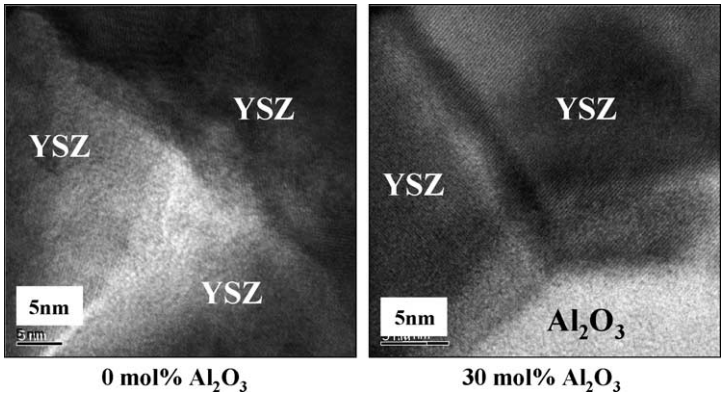


Fig. 6. High magnification TEM micrographs showing triple junctions in 10YSZ–alumina composites containing 0 or 30 mol% alumina.

X-ray diffraction patterns from various 10YSZ–alumina composites are shown in Fig. 1. Cubic zirconia and α-alumina were the only phases present indicating the absence of any chemical reaction between the constituent materials during hot pressing at elevated temperatures. Typical SEM micrographs taken from the polished cross-sections of various YSZ/alumina composites are shown in Fig. 2. Alumina particulates are uniformly dispersed throughout the material. The dark areas represent alumina while the light areas indicate the 10YSZ matrix, as confirmed from EDS analysis (Fig. 3). TEM micrograph and dot maps for various elements for the composite containing 30 mol% alumina are shown in Fig. 4. The average equiaxed grain size is less than 1.0 μm for either YSZ matrix or alumina. The high magnification TEM micrographs showing grain boundaries

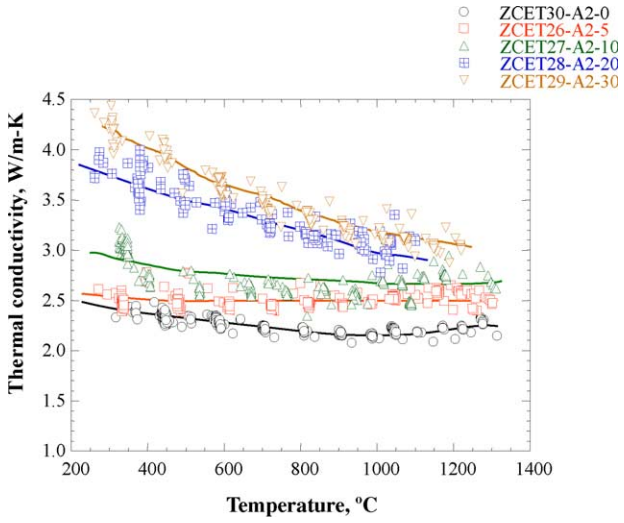


Fig. 7. Temperature dependence of thermal conductivity of 10YSZ–alumina composites containing 0, 5, 10, 20, or 30 mol% alumina determined by a steady-state laser heat flux technique.

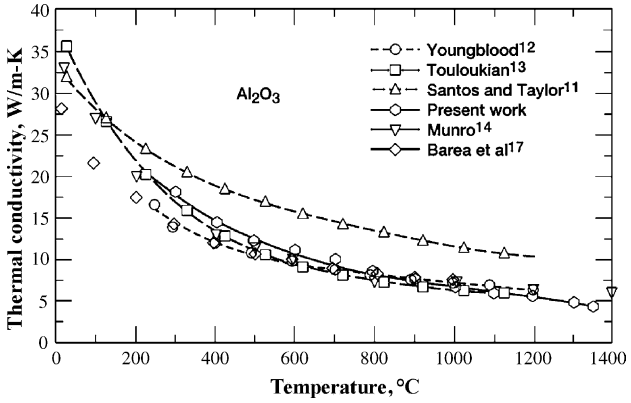


Fig. 8. Thermal conductivity of alumina from various studies (see refs. [13,14,17]).

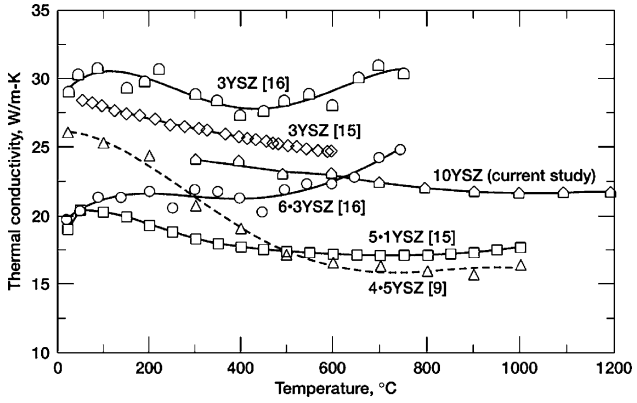


Fig. 9. Thermal conductivity of zirconia containing different mole percent of yttria content (see refs. [9,16]).

and triple junctions for the 0 and 30 mol% alumina composites are presented in Figs. 5 and 6 respectively. The grain boundaries as well as the triple junctions are clean for either composite, indicating the absence of any amorphous phase. No appreciable deformation or microcracks of adjacent grains in the composites, which might occur due to thermoelastic mismatches between the YSZ matrix and the alumina particulates, was observed from the analysis of TEM micrographs.

Thermal conductivities of hot-pressed specimens of 10YSZ–alumina composites of various compositions, as a function of temperature, are shown in Fig. 7. Results for 10YSZ and alumina are also shown for comparison. Data for alumina shows a large scatter particularly in the low temperature region. As alumina has much higher thermal conductivity at low temperatures, the precision of steady-state laser technique, used in the current study, is not as good due to small thermal gradient across the test specimen at low temperatures. Thicker test specimens of alumina may improve the precision. Thermal conductivity increased with increase in alumina content. This is expected, as the thermal conductivity of alumina is much higher [12] than that of 10YSZ. The increase in thermal conductivity with alumina additions is more significant at lower temperatures than at higher temperatures. Thermal conductivity of composites containing 0, 5, and 10 mol% alumina exhibited slight changes with temperature. However, those containing 20 and 30 mol% alumina showed a sharper decrease in thermal conductivity with increase in temperature.

Microstructures of composites of various compositions (Fig. 2) show that alumina phase is uniformly dispersed within the major continuous 10YSZ phase. For materials with such a microstructure, the thermal conductivity of the composite ($k_c$) is given by[10] the Maxwell–Eucken expression:

$$k_c = k_{10YSZ} \frac{\left[(1 + 2V_{Al_2O_3})\left[\frac{(1-k_{10YSZ}/k_{Al_2O_3})}{(1+2k_{10YSZ}/k_{Al_2O_3})}\right]\right]}{\left[(1 - V_{Al_2O_3})\left[\frac{(1-k_{10YSZ}/k_{Al_2O_3})}{(1+k_{10YSZ}/k_{Al_2O_3})}\right]\right]} \quad (2)$$

Table 2
Measured and calculated thermal conductivities of 10YSZ–alumina composites at 1000 °C

| Sample number | Composition (mol%) | | Thermal conductivity (W/m K) at 1000 °C | | |
|---|---|---|---|---|---|
| | 10YSZ | $Al_2O_3$ | Measured (this study) | Calculated from Eq. (2) | Calculated from Eq. (3) |
| A2-0 | 100 | 0 | 2.15 | – | – |
| A2-5 | 95 | 5 | 2.5 | 2.3 | 2.4 |
| A2-10 | 90 | 10 | 2.7 | 2.5 | 2.7 |
| A2-20 | 80 | 20 | 3.0 | 2.9 | 3.2 |
| A2-30 | 70 | 30 | 3.3 | 3.3 | 3.7 |
| $Al_2O_3$ | 0 | 100 | 6.9 | – | – |

where $k_{10YSZ}$ is the thermal conductivity of the continuous phase 10YSZ, $k_{Al_2O_3}$ is the thermal conductivity of the dispersed phase alumina, and $V$ the volume fraction. Thermal conductivity of the composites was also calculated using the simple rule of mixtures:

$$k_c = (k_{10YSZ}V_{10YSZ}) + (k_{Al_2O_3}V_{Al_2O_3}) \quad (3)$$

Thermal conductivity of various 10YSZ–alumina composites at 1000 °C were calculated from Eqs. (2) and (3) using values of 2.15 and 6.88 W/m K for thermal conductivity of 10YSZ and alumina, respectively, measured in the current study. The calculated and measured values are compared in Table 2. For composites containing low mole percent of alumina, the measured thermal conductivities are in reasonable good agreement with those calculated from both Eqs. (2) and (3). However, for higher alumina contents, the measured values of thermal conductivity of 10YSZ–alumina composites are in much better agreement with those calculated from the Maxwell–Eucken model Eq. (2) rather than from the simple rule of mixtures Eq. (3). This is expected based on the microstructures of the composites as shown in Fig. 2.

Thermal conductivity of alumina from various studies is compared in Fig. 8. Results of the present study are in good agreement with those reported by other researchers, particularly at high temperatures. However, values reported by Santos and Taylor [11] are high compared with other studies. Literature values of thermal conductivity of yttria-stabilized zirconia containing various mol% of the stabilizer are shown in Fig. 9, along with the results of the current study for 10 mol% (16.9 wt.%) yttria containing zirconia. Significant variation is seen in the results for different compositions due to different microstructures resulting from various amounts of yttria stabilizer. Thermal conductivity of zirconia decreases with increase in yttria content up to 5.12 mol% (9 wt.%). However, thermal conductivity increased for compositions containing higher yttria content. The 3YSZ consists almost entirely of tetragonal (t) phase [15]. Compositions containing >3 mol% (5.3 wt.%) yttria contain a significant amount of the monoclinic (m) phase and the microstructure consists of a two-phase mixture of t and m phases. The 10YSZ composition of the present study,

containing 10 mol% (16.9 wt.%) yttria, is fully stabilized and consists of the cubic phase of zirconia.

## 5. Summary

Thermal conductivity of 10YSZ–alumina composites containing 0–30 mol% alumina has been determined as a function of temperature using a steady-state laser heat flux technique. Thermal conductivity increased with increase in alumina content. Thermal conductivity showed slight change with temperature for 0, 5, and 10 mol% alumina compositions whereas it decreased with temperature for composites containing 20 and 30 mol% alumina. The measured thermal conductivity values of the 10YSZ–alumina composites are in good agreement with those calculated from the Maxwell–Eucken model where one phase is uniformly dispersed within a second major continuous phase.

## Acknowledgments

This work was supported by NASA's Zero CO2 Emission Technology (ZCET) Project of the Aerospace Propulsion and Power Program. The authors are grateful to John Setlock for processing of the composite materials, Bob Angus for hot pressing, and Ralph Garlick for X-ray diffraction analysis during the course of this research.

## References

[1] N.Q. Minh, Ceramic fuel cells, J. Am. Ceram. Soc. 76 (3) (1993) 563–588.
[2] S.R. Choi, N.P. Bansal, Strength and fracture toughness of YSZ/alumina composites for solid oxide fuel cells, Ceram. Eng. Sci. Proc. 23 (3) (2002) 741–750.
[3] S.R. Choi, N.P. Bansal, Strength, fracture toughness, and slow crack growth of zirconia/alumina composites at elevated temperature, NASA/TM-2003-212108, 2003.
[4] N.P. Bansal, S.R. Choi, Processing of alumina-toughened zirconia composites, NASA/TM-2003-212451, May 2003.
[5] D. Zhu, N.P. Bansal, K.N. Lee, R.A. Miller, Thermal conductivity of ceramic thermal barrier and environmental barrier coating materials, NASA/TM-2001-211122, September 2001.
[6] M. Miyamara, H. Yanagida, A. Asada, Effects of $Al_2O_3$ additions on resistivity and microstructure of yttria-stabilized zirconia, Am. Ceram. Soc. Bull. 64 (4) (1985) 660–664.
[7] F. Ishizaki, T. Yoshida, S. Sakurada, Effect of alumina additions on the electrical properties of yttria doped zirconia, in: S.C. Singhal (Ed.), Proceedings of First International Symposium on Solid Oxide Fuel Cells, The Electrochemical Society, Pennington, NJ, 1989, pp. 3–14.
[8] E.P. Butler, J. Drennan, Microstructural analysis of sintered high-conductivity zirconia with $Al_2O_3$ additions, J. Am. Ceram. Soc. 65 (10) (1982) 474–478.
[9] K. An, K.S. Ravichandran, R.E. Dutton, S.L. Semiatin, Microstructure, texture, and thermal conductivity of single layer and multilayer thermal barrier coatings of $Y_2O_3$-stabilized $ZrO_2$ and $Al_2O_3$ made by physical vapor deposition, J. Am. Ceram. Soc. 82 (2) (1999) 399–406.
[10] W.D. Kingery, H.K. Bowen, D.R. Uhlmann, Introduction to Ceramics, second ed. John Wiley, New York, 1976, p. 636.
[11] W.N.D. Santos, R. Taylor, Effect of porosity on the thermal conductivity of alumina, High Temp.–High Press. 25 (1993) 89–98.
[12] G.E. Youngblood, R.W. Trice, R.P. Ingel, Thermal diffusivity of partially and fully stabilized (yttria) zirconia single crystals, J. Am. Ceram. Soc. 71 (1988) 3255–3260.
[13] Y.S. Touloukian, R.W. Powell, C.Y. Ho, P.G. Clemens, in: Y.S. Touloukian, C.Y. Ho (Eds.), Thermophysical Properties of Solids, vol. 2, Plenum Press, New York, 1970, pp. 93–98.
[14] R.G. Munro, Evaluated material properties for a sintered α-alumina, J. Am. Ceram. Soc. 80 (8) (1997) 1919–1928.
[15] D.P.H. Hasselman, L.F. Johnson, L.D. Bentsen, R. Syed, H.L. Lee, Thermal diffusivity and conductivity of dense polycrystalline $ZrO_2$ ceramic, Am. Ceram. Soc. Bull. 66 (5) (1987) 799–806.
[16] R. Stevens, Zirconia and Zirconia Ceramics, second ed. Magnesium Elekton, Ltd, UK, 1986, 30.
[17] R. Barea, M. Belmonte, M.I. Osendi, P. Miranzo, Thermal conductivity of $Al_2O_3$/SiC platelet composites, J. Eur. Ceram. Soc. 23 (11) (2003) 1773–1778.